DOCUMENT CONTROL SHEET

	ORIGINATOR'S REF. NLR TP 96135 U		SECURITY CLASS. Unclassified

ORIGINATOR
National Aerospace Laboratory NLR, Amsterdam, The Netherlands

TITLE
Vane sweep effects on rotor/stator interaction noise

PRESENTED AT
the 2nd AIAA/CEAS Aeroacoustics Conference, May 6-8, 1996, State College, Pennsylvania, USA

AUTHORS J.B.H.M. Schulten	DATE 960228	pp ref 13 19

DESCRIPTORS

Green's functions	Sweep effect
Interactional aerodynamics	Turbofan engines
Noise reduction	Vanes
Rotor blades	Wakes
Noise generators	Wind tunnel tests
Stator blades	

ABSTRACT
The application of a lifting surface theory to compute the aerodynamic and acoustic response of swept vane stators to viscous rotor wakes is studied. Starting from the flow equations for a perturbed, axially subsonic flow, expressions are derived for the velocity field induced by a stator. A new representation of Green's function is used which avoids the traditional expansion in duct modes. This representation is more practical for arbitrary vane shapes than the classical one. The boundary condition at the vane surface yields an integral equation into a set of linear equations that is solved numerically. The method agrees with the classical method and experimental data for zero sweep. Sample calculations show that vane sweep can be exceptionally effective in the reduction of noise resulting from the interaction of rotor wakes and stator.

NLR TECHNICAL PUBLICATION

TP 96135 U

VANE SWEEP EFFECTS ON ROTOR/STATOR INTERACTION NOISE

by

J.B.H.M. Schulten

Contents

2 Tables
14 Figures

(13 pages in total)

This page is intentionally left blank.

Vane Sweep Effects on Rotor/Stator Interaction Noise

Johan B.H.M. Schulten*

National Aerospace Laboratory NLR, 8300 AD Emmeloord, The Netherlands

The application of a lifting surface theory to compute the aerodynamic and acoustic response of swept vane stators to viscous rotor wakes is studied. Starting from the flow equations for a perturbed, axially subsonic flow, expressions are derived for the velocity field induced by a stator. A new representation of Green's function is used which avoids the traditional expansion in duct modes. This representation is more practical for arbitrary vane shapes than the classical one. The boundary condition at the vane surfaces yields an integral equation for the unknown pressure jump distribution over the vanes. A Galerkin projection transforms this integral equation into a set of linear equations that is solved numerically. The method agrees with the classical method and experimental data for zero sweep. Sample calculations show that vane sweep can be exceptionally effective in the reduction of noise resulting from the interaction of rotor wakes and a stator.

Nomenclature

B	number of blades in row considered
$\bar{c}(\rho)$	axial extent of blade chord
$D(r)$	angular position of zeroth vane, [Eq.(10)]
$g_0(r)$	vector normal to blade helical surface [Eq.(12)]
$H_m^{(2)}$	second kind Hankel function of order m
h	hub/tip ratio
i_x, i_r, i_θ	unit vectors in x,r,θ directions
J_m	Bessel function of the first kind of order m
k	circumferential periodicity of incident velocity
M	axial flow Mach number
$P_{\nu\lambda}$	blade loading coefficient [Eq.(16)]
p	pressure induced by blade row
R_n	reduced Green's function [Eq.(5)]
r	radial coordinate
t	time coordinate
$U_{m\mu}$	radial eigenfunction
v	velocity induced by blade row
W_k	incident velocity with circumferential periodicity
x	axial coordinate along duct axis
α	axial wave number [Eq.(3)]
β	$\sqrt{1 - M^2}$
γ	radial wave number [Eq.(4)]
Δp	blade pressure jump distribution [Eq.(11)]
$\varepsilon_{m\mu}$	radial eigenvalue [Eq.(9)]
θ	circumferential coordinate
ξ	axial source coordinate
ρ	radial source coordinate
τ	source time [Eq.(3)]
ϕ	circumferential source coordinate, local coordinate [Eq.(15)]
Ω	tangential tip Mach number

Subscripts

$()_L$	leading edge
$()_T$	trailing edge

Superscripts

$()^{(a)}$	anechoic
$()^+$	blade lower side
$()^-$	blade upper side
$(\tilde{\ })$	in physical domain

Other Symbol

$\langle \cdot \rangle$	inner product of three-dimensional vectors

Introduction

The interaction of fan wakes and stator outlet guide vanes is the major fan noise mechanism in current high, and future very high, by-pass turbofan engines. To reduce interaction noise, active means have been investigated[1] extensively in recent years. Although some solutions are quite promising, active suppression almost invariably implies delicate and expensive mechanical hardware.

By comparison, passive concepts are relatively simple and some of them, such as acoustic duct lining, have been applied already for a long time. With regard to fan geometry the most famous design rule is Tyler & Sofrin's selection criterion[2] for blade and vane numbers, which is used to achieve a cut-off blade passing frequency in modern fan designs. A large axial gap between fan and outlet guide vanes is also widely appreciated as an effective method of passive noise control. A more sophisticated passive way is to exploit rotor shielding to reflect most of the upstream propagating sound[3]. It is obvious that substantial shielding can only be expected when rotor and acoustic mode rotate in an opposite way. An accurate calculation of the magnitude of this effect requires a method at least at the level of the lifting surface approximation[4]. For the sound propagating downstream from the outlet guide vanes the absence of such shielding is a matter of increasing concern with regard to the emerging very high by-pass fans.

In a more general sense, passive noise control is equivalent to the design of inherently quiet fans. It therefore requires a fairly complete modeling of the sound generation process. Calculation is necessary since intuition easily fails as was shown for leaned vanes[5], which in general seem not to

*Senior Research Engineer, Aeroacoustics Department, Senior Member AIAA.

provide a viable way to sound reduction.

Vane sweep is used in many fan designs to influence the sound production. However, not until 1989 an unsteady lifting surface method for a rotor with swept blades was published by Kodama and Namba[6] to quantify this effect. They found favorable effects of blade sweep on the acoustic response to sinusoidal gust interaction. However, in the pursuit of a quiet fan it is more natural to look at the stator vanes which have less mechanical constraints than the rotor blades.

Lifting surface methods have been shown to be very useful in the calculation of interaction sound (Namba[7], Kobayashi & Groeneweg[8], Lordi & Homicz[9], Salaün[10], Schulten[11]). These methods have the outstanding advantage of being fully consistent with the level of approximation of linear duct acoustics, still the favored model for high frequency acoustic lining optimization. Also, the physically important ratio of blade row dimensions and the acoustic and hydrodynamic wavelengths involved is conserved in the lifting surface approximation.

Compared to Euler and Navier-Stokes methods the absence of numerical dissipation or dispersion in the lifting surface methods, their exactness and their, by comparison, short computation times make them very suitable for optimization of blade and vane geometries. They also can provide limiting test cases to compare results of numerical methods with. A further advantage is that, by their analytical nature, isolated effects can, in general, be traced more precisely. A drawback may be the mathematical complexity of the formulations and, of course, their inherent limitation to small perturbations.

The basic result of any lifting surface method is the pressure jump distribution over the blades or vanes. Once the pressure jump distribution is known, it is only a minor effort to compute the steady and unsteady pressure or velocity fields generated by the blade row.

In the present paper a lifting surface method is applied to swept stator vanes. The method is based on a new representation of the Green's function[12] which is basically an extension of the Fourier-expansion of the free-space Green's function for propellers to include the sound reflections on hub and casing. The method is validated with experimental results of the NLR rotor/stator interaction model[13] and with results of the classical method for unswept vanes. For this configuration the effects of a progressive vane sweep angle on first and second harmonic of the interaction sound are studied. The numerical accuracy of the method is checked by varying the number of basis functions that describe the vane pressure jump distribution. Further, the potential of vane sweep for a typical high speed fan geometry is numerically explored.

Analysis

Governing equations

A lifting surface modeling of a flow problem is based on two assumptions. First, the viscosity of the flow is considered to be small, i.e. the Reynolds number is assumed to be sufficiently high. Secondly, the perturbations of the main flow caused by the presence of the blades are supposed to be relatively small.

We consider a single blade row placed in a uniform, subsonic main flow of Mach number M ($0 < M < 1$). To obtain a non-dimensional formulation, the mass density and speed of sound of the main flow and the duct radius are taken as scaling parameters. With this scaling the pressure and density perturbation become to leading order identical. If the x-axis is chosen along the duct axis, the governing, i.e. the leading order, flow equations are the linearized Euler equations for the (dimensionless) perturbation pressure $\tilde{p}$ and velocity $\tilde{v}$

$$\frac{D\tilde{p}}{Dt} + \langle \nabla \cdot \tilde{v} \rangle = 0 \tag{1}$$

and

$$\frac{D\tilde{v}}{Dt} + \nabla\tilde{p} = 0 , \tag{2}$$

where the linearized material derivative $D/Dt = \partial/\partial t + M\partial/\partial x$. A tilde indicates that the variable is understood to be in the physical domain.

As shown previously[14,15], application of generalized functions to make Eqs.(1-2) formally valid throughout space, i.e. also within the blades, and elimination of the velocity yields a non-homogeneous convected-wave equation in the pressure. The right hand side of this equation consists of two source terms, one of which contains the blade loading distribution and the other the blade thickness distribution. After the construction of a Green's function for this equation in terms of a multiple Fourier transform, the pressure field of the complete blade row can be expressed as an integral over a volume that contains the blade row. This pressure field contains both steady and unsteady, acoustic components at multiples, including zero, of the blade passing frequency. Upon substitution of the pressure field, the momentum equation yields expressions for the velocity induced by blade displacement and the blade loading velocity.

Green's function

In this section we will construct $\bar{G}$ as the superposition of Green's function in free space and cylindrical waves reflected by the hub and the casing. This is possible by representing $\bar{G}$ as a superposition of circumferential and axial waves in the following multiple wave spectrum

$$\bar{G}(x,r,\theta,t|\xi,\rho,\phi,\tau) = \frac{1}{(2\pi)^3} \sum_{n=-\infty}^{\infty} \exp[in(\theta-\phi)]$$

$$\times \int_{-\infty}^{\infty}\int_{-\infty}^{\infty} \exp[i\{\omega(t-\tau)+\alpha(x-\xi)\}] R_n(\alpha,r,\omega|\rho)\,d\alpha\,d\omega , \tag{3}$$

where R_n is a 'reduced Green's function', defined hereafter. In this formulation chordwise integrals can be easily taken since the axial source coordinate ξ only occurs directly in an exponential. Now we introduce the radial wave number γ which is related to the axial wave number α and the Helmholtz number (dimensionless frequency) ω as

$$\gamma^2 = (\omega + M\alpha)^2 - \alpha^2 . \tag{4}$$

If the branch cuts of γ are taken such that $\text{Im } \gamma \leq 0$ throughout the complex α-plane, the anechoic, free space reduced

Green's function is given by[12]

$$R_n^{(a)} = -i\frac{\pi}{2}\left[J_n(\gamma r)H_n^{(2)}(\gamma\rho)\,\mathrm{H}(\rho-r)\right.$$

$$\left. + J_n(\gamma\rho)H_n^{(2)}(\gamma r)\,\mathrm{H}(r-\rho)\right] \tag{5}$$

where H denotes the Heaviside unit step function. In the present case of a cylindrical duct the hard wall boundary condition $\partial R_n/\partial r = 0$ at the hub $(r = h)$ and at the casing $(r = 1)$ is satisfied by adding the reflected cylindrical waves. Therefore we presume

$$R_n = R_n^{(a)} + A\,H_n^{(2)}(\gamma r) + B\,J_n(\gamma r) \tag{6}$$

Sine the added cylindrical waves satisfy the Bessel equation, they do not affect the right hand side in the equation for the Green's function[12]. Application of the boundary conditions at hub and casing determines the coefficients A and B and we obtain

$$R_n = R_n^{(a)} + i\frac{\pi}{2}\,\frac{1}{J_n'(\gamma)H_n^{(2)'}(\gamma h) - J_n'(\gamma h)H_n^{(2)'}(\gamma)}$$

$$\times\left\{\left[J_n'(\gamma)\,H_n^{(2)}(\gamma\rho) - H_n^{(2)'}(\gamma)J_n(\gamma\rho)\right]J_n'(\gamma h)H_n^{(2)}(\gamma r)\right. \tag{7}$$

$$\left. -\left[J_n'(\gamma h)H_n^{(2)}(\gamma\rho) - H_n^{(2)'}(\gamma h)J_n(\gamma\rho)\right]H_n^{(2)'}(\gamma)J_n(\gamma r)\right\}$$

The reason to avoid the more natural combination of Hankel functions of the first and second kind in Eq.(6) , or alternatively Bessel functions of the first and second kind, is that this would lead to subtraction of very large terms in certain parts of the α-plane with subsequent fatal loss of numerical accuracy.

After rearrangement of Eq.(7) it is possible to recover the traditional Green's function by performing the Fourier integral to α, which comes down to summation of the residues. Then the classical Green's function representation in duct modes given by

$$\tilde{G} = \frac{1}{(2\pi)^2}\int_{-\infty}^{\infty}\exp[i\omega(t-\tau)]\sum_{n=-\infty}^{\infty}\exp[in(\theta-\phi)]\sum_{\mu=1}^{\infty}U_{n\mu}(r)$$

$$\times\frac{U_{n\mu}(\rho)}{2i\beta_{n\mu}(\omega)}\exp\left[i\frac{(x-\xi)}{\beta^2}[M\omega - \mathrm{sgn}(x-\xi)\beta_{n\mu}(\omega)]\right]d\omega \tag{8}$$

results. Here the square root $\beta_{n\mu}$ is defined as

$$\beta_{n\mu} = \omega\sqrt{1 - (\varepsilon_{n\mu}\beta/\omega)^2} \quad \text{if } (\varepsilon_{n\mu}\beta)^2 \le \omega^2$$

$$\beta_{n\mu} = -i\sqrt{(\varepsilon_{n\mu}\beta)^2 - \omega^2} \quad \text{if } (\varepsilon_{n\mu}\beta)^2 > \omega^2 \tag{9}$$

where the radial eigenvalues are denoted by $\varepsilon_{n\mu}$.
Not only Green's function but any sound field in a duct can be described in terms of a superposition of duct modes. If $\beta_{n\mu}(\omega)$ is real, the mode is said to be 'cut-on' since it propa-

gates without attenuation along the duct in upstream and downstream direction. If, on the other hand, $\beta_{n\mu}(\omega)$ is imaginary, the mode is 'cut-off' because it is exponentially decaying from the source. Each mode has its particular cut-off frequency given by $\pm\beta\varepsilon_{n\mu}$. This classical representation of Green's function has been used in all lifting surface methods for ducted fans thus far. Its main disadvantage is the highly oscillating character of the large order eigenfunctions $U_{n\mu}$ [Fig.1], which leads to a cumbersome numerical integration in the blades spanwise direction.
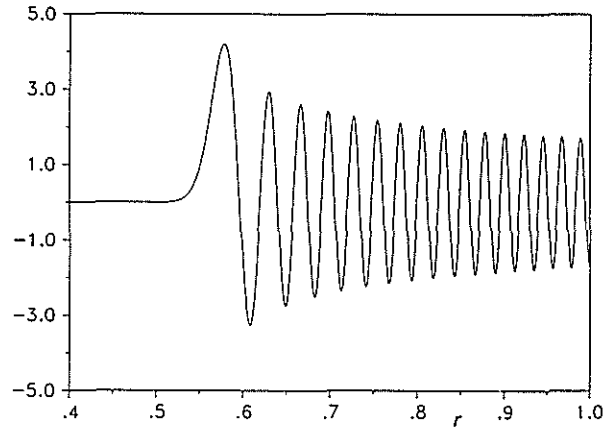

Fig. 1   Example of radial eigenfunction $U_{n\mu}(r)$, $n=200$, $\mu=32$, $h=0.4$

Until recently[6], the traditional expansion of Green's function into duct modes[7,8,9,10] has only been applied to ducted blade rows of the most simple geometry, i.e. leading and trailing edges in cross-sectional planes. The reason for this is that the infringement on the separation of variables by swept or tapered blades increases the complexity as well as the computational effort dramatically. If only the field upstream or downstream of a blade row is to be described, the classical Green's function is the more efficient vehicle. Then, the complete sound field in a duct can be described to high accuracy by a relatively small number of duct modes, viz. the cut-on modes supplemented with a few cut-off modes. However, in a lifting surface problem high order cut-off modes play a much more important role than they do at some axial distance from the blade row. The present formulation [Eq.(3)], in which the summation over radial modes has been replaced by an integral, accepts blades of a general planform, i.e. with leading and trailing edges that are a function of the radius, without significant penalty in complexity. Therefore, it seems much better suited to study effects as blade sweep and taper on the sound generation process of ducted fans.

Blade loading velocity field

As shown in Ref.14, substitution of the actual force field exerted by the blades into the expression for the velocity leads, after some algebra, to the following expression for the velocity induced by a blade row

$$\bar{v}_F = \frac{B}{(2\pi)^3 M} \sum_{n=-\infty}^{\infty} \int_{-\infty}^{\infty} \exp(i\omega_m t)\exp(im\theta)$$

$$\times \int_{-\infty}^{\infty} \frac{\exp(i\alpha x)}{i(\alpha + \frac{\omega_m}{M})} \left. \int_h \rho \exp[-imD(\rho)] \right\} g_0(\rho)\frac{\delta(r-\rho)}{r}$$

$$(10)$$

$$- \begin{bmatrix} \alpha \\ -i\partial/\partial r \\ m/r \end{bmatrix} \left\langle g_0(\rho) \cdot \begin{bmatrix} \alpha \\ i\partial/\partial\rho \\ m/\rho \end{bmatrix} \right\rangle R_m(\alpha,r,\omega_m|\rho)$$

$$\times \int_{x_L(\rho)}^{x_T(\rho)} \exp[i(\frac{m\Omega}{M}-\alpha)\xi]\Delta p(\xi,\rho,\omega)\,d\xi\,d\rho\,d\alpha\,d\omega$$

where $\omega_m = \omega - m\Omega$ and $m = k - nB$. For the sake of completeness this expression is for a rotor. For a stator it simplifies because then $\Omega=0$. The pressure jump distribution is defined as

$$\Delta p(\xi,\rho,\omega) = p^+(\xi,\rho,\omega) - p^-(\xi,\rho,\omega) \qquad (11)$$

and the vector normal to the undisturbed helical surfaces

$$g_0(r) = \frac{\Omega}{M}i_x - D'(r)i_r + \frac{1}{r}i_\theta \, , \qquad (12)$$

For stator vanes without lean a further simplification is that $D'=0$ in Eq.(12).

Integral equation
The only unknown quantity in the expression of the blade loading velocity [Eq.(10)] is the blade pressure jump distribution Δp. To solve Δp we have to apply the boundary condition of flow tangency at the blade surfaces. This boundary condition is rewritten in such a way that the right hand side depends solely on known quantities. By splitting the incident field into circumferential Fourier components $\bar{W}_k(x,r,t)$ exp$(ik\theta)$, the integral equation has to be solved for one blade only. Combining the boundary conditions at upper and lower blade surfaces as in Ref.12 we obtain the following integral equation for Δp due to an incident velocity field

$$\left[\langle g_0 \cdot \bar{v}_F \rangle = - \langle g_0 \cdot \bar{W}_k e^{ik\theta} \rangle \right]_{\theta = \Omega + \Omega(t - x/M)} \qquad (13)$$

Numerical Solution Procedure
The first step towards the numerical solution of the integral equation [Eq.(13)] is the choice of a suitable description of the unknown pressure jump distribution. In principle this can be achieved by approximating Δp by a finite set of basis functions, also called loading or trial functions. Since vanes operate definitely in the subsonic regime, an appropriate choice for the chordwise representation is[12]

$$\Delta p = P_0(\rho)\tan\frac{\phi}{2} + \sum_{\lambda=1}^{\lambda_{max}} P_\lambda(\rho) \sin\lambda\phi \qquad (14)$$

where ξ is related to ϕ by

$$\xi = \frac{x_T(\rho)+x_L(\rho)}{2} + \frac{\bar{c}(\rho)}{2}\cos\phi \, . \qquad (15)$$

This representation incorporates the usual subsonic square root leading edge singularity as well as a Kutta condition behavior at the trailing edge. It also permits the chordwise integrals in Eq.(10) to be evaluated analytically, a most welcome computer time saving quality, which is missed with the classical Green's function representation.

In the spanwise direction $P_\lambda(\rho)$ is expanded in a Chebyshev series as follows

$$P_\lambda(\rho) = \sum_{\nu=0}^{\nu_{max}} P_{\nu\lambda} \cos\nu\psi \qquad (16)$$

where

$$\cos\psi = 2(\rho-h)/(1-h) - 1 \, . \qquad (17)$$

Now a Galerkin projection as described in Ref.16 transforms the integral equation into a system of linear equations that can be solved by standard matrix techniques.

Table 1 Low speed configuration

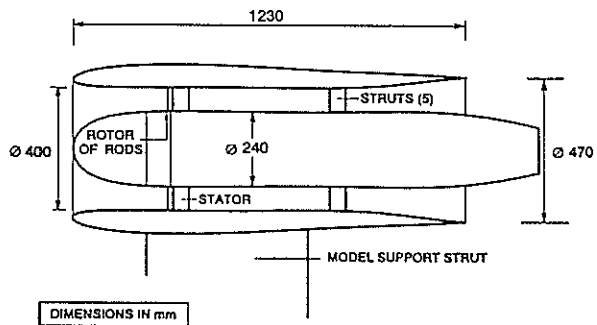|	
Number of rotating rods	16
Number of stator vanes	18
Hub/tip ratio, h	0.6
Axial vane chord length	0.25
Axial Mach number	0.244
Rods circumferential tip Mach number	0.406
Rods drag coefficient	1.2
Nondimensional 1st harmonic frequency	6.491
Speed of sound (m/s)	340.43
Air density (kg/m^3)	1.225

Fig. 2 NLR fan noise wind tunnel model

Experimental validation

To validate the new method it was applied to a standard experimental NLR test case. Fig.2 shows the experimental model[11,13] consisting of a through-flow nacelle with a 0.4 m diameter duct, which was installed in a low speed wind tunnel. A 0.24 m diameter hub formed the inner boundary of the annular geometry in which a stator with 18 unswept vanes was installed. In front of the stator a rotor consisting of 16 cylindrical rods (diameter 3 mm) was mounted. These rods were used as acoustically transparent wake generators to produce a periodic velocity perturbation field.
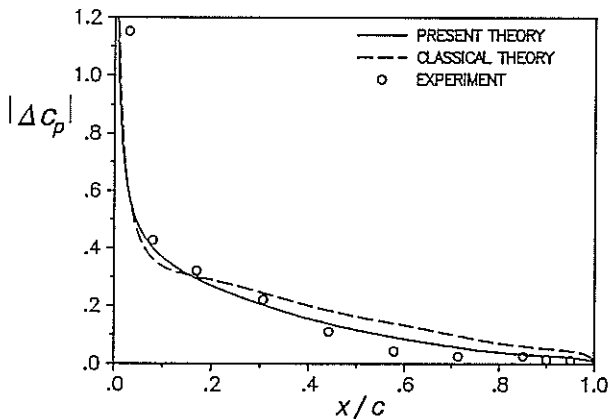
Fig. 3 Comparison of two lifting surface methods with NLR fan experiment [Ref.13], 1st Harmonic, r = 0.8 (mid span), conditions in Table 1.
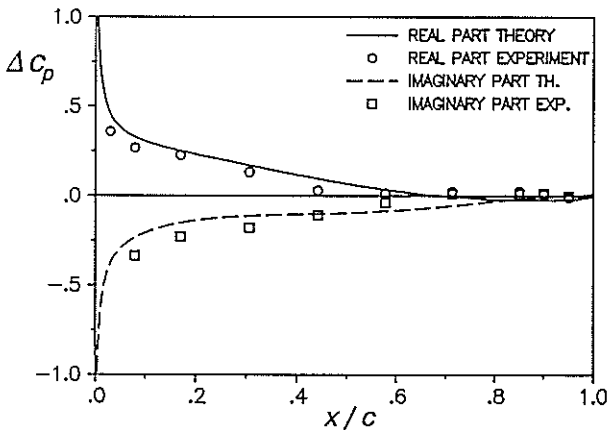
Fig. 4 Mid span pressure jump distribution, 1st harmonic, conditions in Table 1.

The comparison of the new lifting surface method and the classical one for the NLR fan experiment is made in Fig.3. Obviously the absolute values of the pressure jump distributions of both lifting surface methods are close, with the classical one showing a slightly larger discrepancy with the experiment. It is to be noted that differences between the two methods are entirely due to differences in the numerical treatment and subsequent programming, since the methods are analytically equivalent. The agreement with the experiment is surprisingly good, bearing in mind that in this case the

disturbance level is as high as 20 percent of the free-stream velocity, which can be hardly considered to be a small perturbation. Fig.4 shows a complex representation of the pressure jump distribution, measured and computed with the present theory. It appears that also the phase is accurately predicted. For this comparison use was made of the measured wake velocities to obtain the right hand side of Eq.(13). It was found that Schlichting's wake formulas[17] give a good description of these wakes. Therefore these formulas were used in the next numerical examples for swept vanes.

Numerical examples

Low speed configuration

The NLR fan experiment was taken as a starting point for an exploratory study of the effects of vane sweep. For the 1st harmonic of the rod wake system, lifting surface calculations were made for sweep angles up to 30 degrees at five degree intervals. The vane intersection with the hub was kept in place while the intersection with the casing followed from the sweep angle [Fig.5, Table 1]. This way the vane area was kept constant.
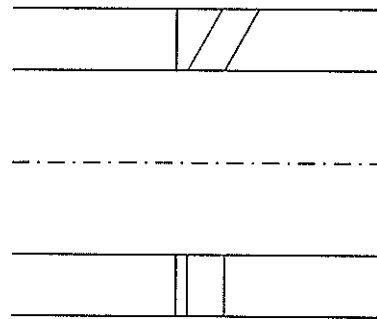

Fig. 5 Low speed interaction model with rotating rods and unswept vanes (lower); 30 deg swept vane configuration as computed (upper), conditions in Table 1.
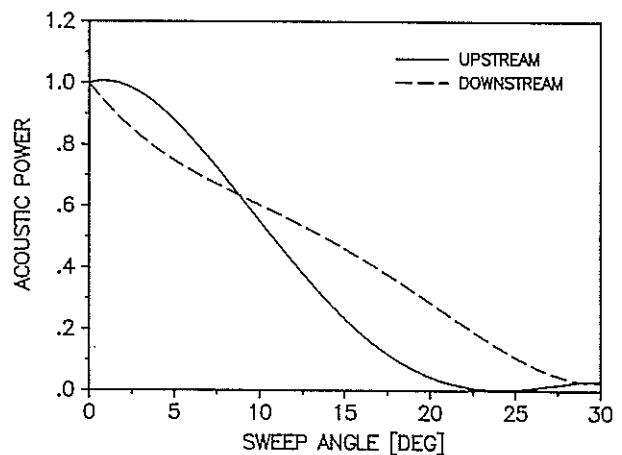

Fig. 6 Normalized acoustic power of 1st harmonic, conditions in Table 1.

1st Harmonic Fig.6 shows the effect of the first harmonic upstream and downstream acoustic power, normalized on their values at zero sweep. Since in this case only one mode is cut-on at the 1st harmonic ($m=2,\mu=1$) this is also the modal power. Clearly, the upstream power virtually disappears beyond 20 deg. of sweep. The downstream power falls slower but at a sweep angle of 28 deg. also the downstream power has effectively vanished.
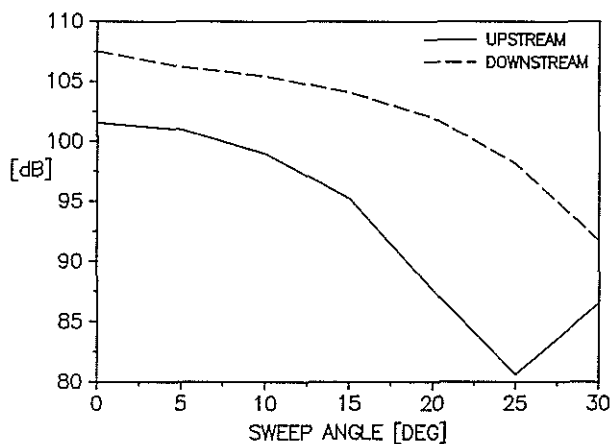

Fig. 7 Acoustic intensity level 1st harmonic, conditions in Table 1.

The difference in upstream and downstream behavior is a consequence of the difference in the modal axial wavelength as can be seen in the expression for the pressure induced by the loading of an unleaned vane

$$\tilde{p}_L(x,r,\theta,t) = \frac{-B}{2\pi}\exp(i\omega t) \sum_{n=-\infty}^{\infty} \exp[im(\theta-D)]$$

$$\times \sum_{\mu=1}^{\infty} \frac{U_{m\mu}(r)}{2\beta_{m\mu}(\omega)} \left| \frac{m}{\rho} U_{m\mu}(\rho) \right.$$ (18)

$$\times \int_{x_l(\rho)}^{x_t(\rho)} \exp\left[i\frac{(x-\xi)}{\beta^2}[M\omega-sgn(x-\xi)\beta_{m\mu}(\omega)] \right] \Delta p(\xi,\rho)\,d\xi\,d\rho$$

In the present case $\beta_{2,1}=6.015$ which yields an upstream wave number of 7.599 and a downstream wave number of -4.431. Since these wave numbers occur also in the exponential in the chordwise integral in Eq.(18) it may be clear that the upstream mode is almost twice as sensitive to an axial source variation as the downstream mode. So it is indeed to be expected that the upstream mode more directly responds to vane sweep than the downstream mode with its longer wavelength.

Fig.7 shows the acoustic intensity level in dB (reference 10^{-12} watt/m²). It is observed that the downstream level is considerably higher than the upstream level. Since the upstream propagating sound can also be reduced by rotor shielding, it is the downstream sound that would need all attention in this case. It is obvious that impressive sound reductions of more than 15 dB can be achieved both upstream and downstream even with a simple constant sweep angle. It may be noted that
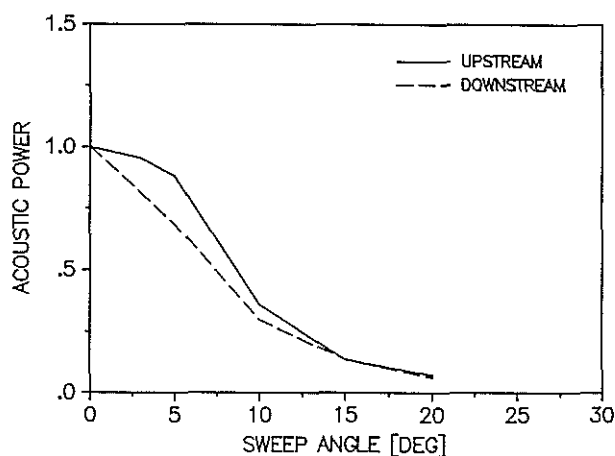

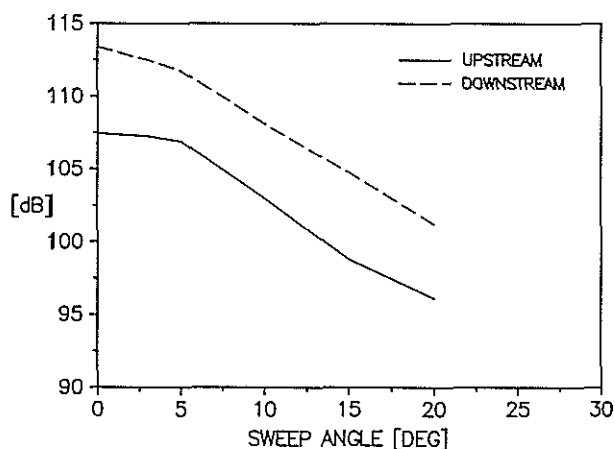Fig. 8 Normalized acoustic power 2nd harmonic, conditions in Table 1.

Fig. 9 Acoustic intensity level 2nd harmonic, conditions in Table 1.

the reduction is of the same order as recently reported by Kerschen & Reba[18] for active control leading edge actuators.
2nd Harmonic In Fig.8 the normalized acoustic power of the second harmonic is shown. At this frequency two modes with circumferential periodicity $m=4$ are cut-on. For the upstream power it takes about 5 degrees of sweep before it starts to fall. The downstream power directly starts to decrease but beyond 15 degrees the upstream and downstream sound reductions are practically equal. As shown in Fig.9, a 10 dB reduction is attained at 20 degrees. Note that the overall intensity level sound is higher than it was for the first harmonic. Also, the downstream level is again considerably higher than the upstream.
Numerical validation of method To check the numerical accuracy of the method, the number of basis functions representing the pressure jump distribution was systematically varied. The number of basis functions strongly affects the required computing time and normally one should avoid an overdose of basis functions. The second harmonic of the low speed cas e just discussed was used as a test case. Fig.10 presents the computed intensity level for a sweep angle of 20

degrees as a function of the number of chordwise basis functions. The number of spanwise basis functions was kept constant at 11 ($=\nu_{max}+1$). It appears that beyond $\lambda_{max}=6$ the computed intensity level is practically constant.

The same exercise was done for the spanwise basis functions while the number of chordwise functions was kept at 14 ($=\lambda_{max}+1$). For this case it is clear that $\nu_{max}=7$ is sufficient for a correct result.

It must be noted that these figures are very much case-related. In particular a different frequency, chord length and hub/tip ratio (h) will change the minimum required number of basis functions.
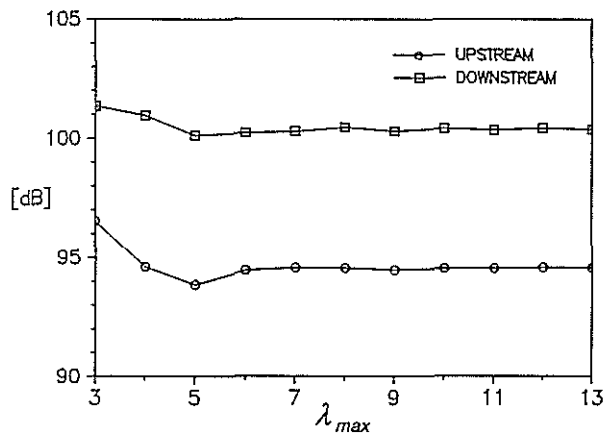

Fig. 10   Effect of the number of chordwise basis functions, sweep angle 20 deg, $\nu_{max}=10$, 2nd harmonic, conditions in Table 1.
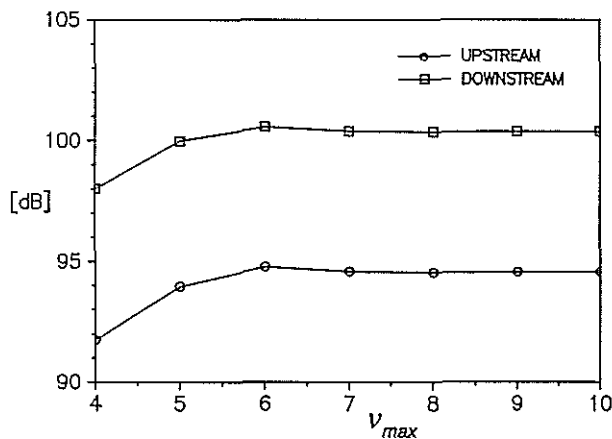

Fig. 11   Effect of number of spanwise basis functions, $\lambda_{max}=13$, 2nd harmonic, conditions in Table 1.

High speed fan

Although the previous example had the advantage of a direct relation to a well-documented experiment, the real interest of the method is of course in its application to the emerging very high bypass turbofans. Inspired by the Advanced Ducted Propeller (ADP) experiment by Woodward et al.[19], a high speed fan configuration was defined, as given in Table 2 and Fig.12. As usual for modern fans, the 1st harmonic is cut-off.

Table 2   High speed fan example

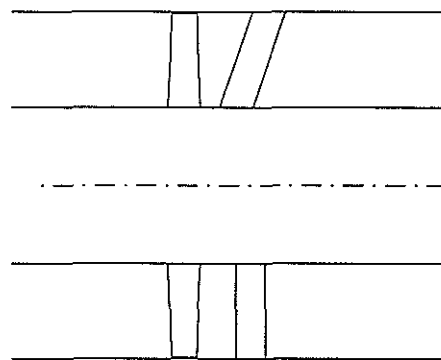| Number of rotor blades	16
Number of stator vanes	40
Hub/tip ratio, h	0.45
Initial vane chord length	0.17
Mid span axial gap	0.219
Axial Mach number	0.288
Rotor circumferential tip Mach number	0.76
Rotor blade drag coefficient	0.01
Nondimensional 2nd harmonic frequency	24.32
Speed of sound (m/s)	340.43
Air density (kg/m^3)	1.225

Fig. 12   High speed fan geometry; 20 deg swept vane (upper) and unswept vane (lower), see also Table 2.

In the 2nd harmonic four modes with circumferential periodicity $m=8$ are cut-on. The nondimensional frequency of this case is almost twice as high as in the previous example. The rotor chord was taken as

$$c(r) = 0.247 \sqrt{1 + [(2r/(1+h)]^2} \tag{19}$$

With a constant rotor blade drag coefficient of 0.01 the turbulent, viscous wakes were computed in a quasi-two-dimensional way[12,17] to provide the incident velocity field in Eq.(13).

A serious point of criticism that could be raised against the previous example is the fact that by sweeping the vane backward the average distance of vane leading edge and rods increases considerably (Fig.5). So one could argue that it is not so much the sweep but rather the increased gap that is responsible for the sound reduction. Although it is obvious that a larger gap has a beneficial effect on the sound production, it is not plausible that this effect alone could be so strong. To avoid, however, the mixture of these two effects, in the present example the midspan axial gap was kept constant, i.e. the mid span leading edge point was hold in place as the sweep angle was varied [Fig.12].

Here, the axial gap itself was taken smaller than would be typical in an actual ADP design to prevent a completely merged viscous wake system with a rather unpredictable residual structure. It may be expected that for a large gap it

is the inviscid wake system of the fan that dominates the incident velocity field at the vanes. The present viscous wake system should therefore be considered only as a sample to demonstrate the effect of vane sweep for a well-organized incident field.

Another point of concern is the loss of steady aerodynamic loading of a swept vane. For a high aspect ratio vane the aerodynamic performance depends on the velocity component normal to the leading edge rather than on the total velocity. To preserve the aerodynamic performance the axial vane chord was varied with the sweep angle as

$$c = c_0 / \cos^2 \lambda \qquad (20)$$

where c_0 is the initial chord at zero sweep and λ is the sweep angle. As a result also the vane surface increases with the sweep angle (Fig.12).
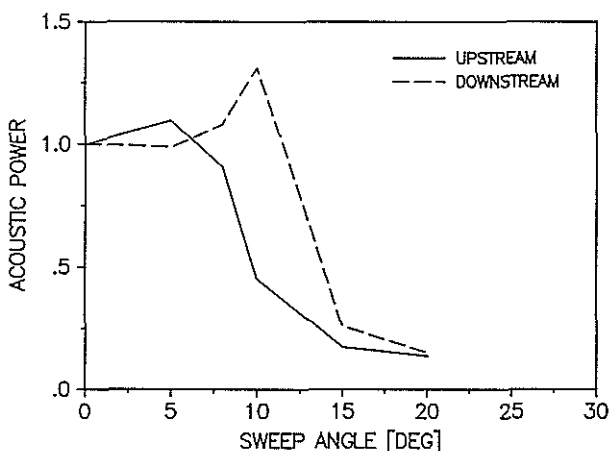
Fig. 13 Normalized Acoustic Power, 2nd harmonic, conditions in Table 2.
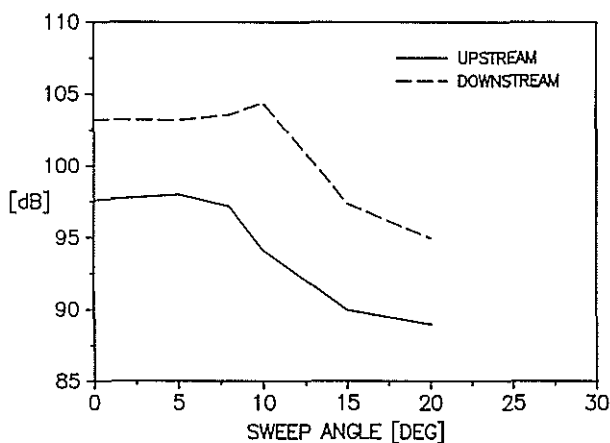
Fig. 14 Acoustic intensity level, 2nd harmonic, conditions in Table 2.

It is shown in Fig.13 that sweep does not yield immediate benefits for this configuration. On the contrary, first some critical value has to be passed before a sharp decrease starts. The upstream sound starts to decrease earlier than the downstream sound which requires about 12 deg to become lower

than its zero sweep level. So a too small sweep angle may have an adverse effect. As shown in Fig.14 still considerable sound reductions in the order of 8 dB are possible with 20 deg of sweep. The downstream intensity level is again considerably higher than the upstream level.

Concluding remarks

The application of a lifting surface method to the calculation of aerodynamic and acoustic response of swept stators to impinging rotor wakes has been discussed.

A new element in the present method is the representation of the Green's function as an integral instead of the more familiar infinite sum of radial modes. The method can be considered as an extension of a propeller lifting surface formulation.

Comparison with experimental data and results of the classical Green's function formulation shows the validity of the new method. The numerical consistency of the method has been checked by systematically varying the representation of the unsteady vane pressure jump distribution.

Calculations for the experimental NLR fan model for a range of sweep angles up to 30 degrees show a potential of 10 to 15 dB noise reduction.

At conditions relevant for a modern, very high bypass design interaction noise reductions in the order of 8 dB seem to be obtainable with 20 deg of vane sweep. Smaller sweep angles may cause a sound increase.

The found effectiveness of a simple backward vane sweep invites to further research into forward sweep and more sophisticated, curved vane planforms.

For the same sweep angle, the computed downstream noise levels persistently appear to be considerably higher than upstream levels.

References

[1]Simonich, J.C., "A Review of Actuators for Active Noise Control in Gas Turbines," CEAS/AIAA Paper 95-059, June 1995.

[2]Tyler, J.M., Sofrin, T.G., "Axial Flow Compressor Noise Studies," SAE Transactions, Vol. 70, 1962, pp. 309-332.

[3]Smith, M.J.T., Aircraft Noise, Cambridge University Press, 1989

[4]Schulten, J.B.H.M., "Transmission of Sound through a Rotor," DGLR/AIAA Paper 92-02-085, May 1992.

[5]Schulten, J.B.H.M., "Sound Generated by Rotor Wakes Interacting with a Leaned Vane Stator," AIAA Journal, Vol.20, No.10, 1982, pp.1352-1358.

[6]Kodama, H., Namba, M., "Unsteady Lifting Surface Theory for a Rotating Cascade of Swept Blades", ASME Paper 89-GT-306, June 1989.

[7]Namba, M., "Three-Dimensional Analysis of Blade Force and Sound Generation for an Annular Cascade in Distorted Flows," Journal of Sound and Vibration, Vol.50, No.4, 1977, pp.479-508.

[8]Kobayashi H., Groeneweg, J.F., "Effects of Inflow Distortion Profiles on Fan Tone Noise," AIAA Journal, Vol. 18, No. 8, 1980, pp. 899-906.

[9]Lordi, J.A., Homicz, G.F., "Linearized Analysis of the Three-Dimensional Compressible Flow through a Rotating Annular Blade Row," *Journal of Fluid Mechanics*, Vol.103, 1981. pp. 413-442.

[10]Salaün, P., "Unsteady Aerodynamic Pressures on an Annular Cascade in Subsonic Flow," (in French), ONERA Publ.No.158, 1974. Translated in English as European Space Agency Tech. Transl., ESA-TT-173, 1975.

[11]Schulten, J.B.H.M., "Experimental Validation of a Lifting Surface Model for Rotor Wake - Stator Interaction," AIAA Paper 89-1125, April 1989.

[12]Schulten, J.B.H.M, "Sound Generation by Ducted Fans and Propellers as a Lifting Surface Problem," Ph.D. Thesis, University of Twente, Enschede, The Netherlands, Feb. 1993.

[13]Zandbergen, T., "Stator Vane Response due to the Impingement of the Wake of an Unloaded Rotor," AIAA Paper 88-2814, July 1988.

[14]Schulten, J.B.H.M., "Effects of Asymmetric Inflow on Near-Field Propeller Noise," *AIAA Journal*, Vol.34, No.2, Feb. 1996, pp. 251-258.

[15]Ffowcs Williams, J.E., Hawkings, D.L., "Sound generation by turbulence and surfaces in arbitrary motion," *Philosophical Transactions of the Royal Society of London*, Series A, Vol.264, 1969, pp. 321-341.

[16]Schulten, J.B.H.M., "Advanced Propeller Performance Calculation by a Lifting Surface Method," AIAA Paper 95-3035. July 1995, accepted for publication in the *Journal of Propulsion and Power*.

[17]Schlichting, H., *Boundary Layer Theory*, McGraw-Hill, New York, 1979.

[18]Kerschen, E.J., Reba, R.A., "Active Control of Wake-Airfoil Interaction Noise by Leading Edge Actuators," CEAS/AIAA paper 95-058, June 1995.

[19]Woodward, R.P., Bock, L.A., Heidelberg, L.J., Hall, D.G., "Far-Field Noise and Internal Modes From a Ducted Propeller at Simulated Takeoff Conditions," AIAA Paper 92-0371, January 1992.